Chemical Engineering Journal 111 (2005) 225–236

Chemical Engineering Journal

www.elsevier.com/locate/cej

Permeability–porosity relationship from a geometrical model of shrinking and lattice Boltzmann and Monte Carlo simulations of flow in two-dimensional pore networks

Javier R. Quispe [a], Roberto E. Rozas [b], Pedro G. Toledo [c,*]

[a] *School of Environmental Science and Engineering, Catholic University of Temuco, PO Box 15-D, Temuco, Chile*
[b] *Institut für Physikalische Chemie, Universität zu Köln, Luxemburger Str. 116, 50939 Köln, Germany*
[c] *Chemical Engineering Department, Surface Analysis Laboratory (ASIF), University of Concepción, PO Box 160-C, Correo 3, Concepción, Chile*

Abstract

For a broad range of applications, the most important transport property of porous media is permeability. Here we calculate the permeability of pore network approximations of porous media as simple diagenetic or shrinking processes reduces their pore spaces. We use a simple random bond-shrinkage mechanism by which porosity is decreased; a tube is selected at random and its radius is reduced by a fixed factor, the process is repeated until porosity is reduced either to zero or a preset value. For flow simulations at selected porosity levels, we use precise Monte Carlo calculations and the lattice Boltzmann method with a 9-speed model on two-dimensional square lattices. Calculations show a simple power-law behavior, $k \propto \phi^{m}$, where k is the permeability and ϕ the porosity. The value of m relates strongly to the shrinking process and extension, and hence to the skewness of the pore size distribution, which varies with shrinking, and weakly to pore sizes and shapes. Smooth shrinking produces pore space microstructures resembling the starting primitive material; one value of m suffices to describe k versus ϕ for any value of porosity. Severe shrinking however produces pore space microstructures that apparently forget their origin; the k–ϕ curve is only piecewise continuous, different values of m are needed to describe it in the various porosity intervals characterizing the material. The power-law thus is not universal, a well-known fact. An effective pore length or critical pore size parameter, l_c, characterizes pore space microstructures at any level of porosity. For severe shrinking l_c becomes singular, indicating a change in the microstructure controlling permeability, and thus flow, thus explaining k–ϕ power-law transitions. Continuation of the various k–ϕ pieces down to zero permeability reveals pseudo-percolation thresholds ϕ'_c for the porosity of the controlling microstructures. New graphical representations of k/l_c^2 versus $\phi - \phi'_c$ for the various ϕ intervals display straight and parallel lines, with a slope of 1. Our results confirm that a universal relationship between k/l_c^2 and ϕ should not be discarded.

Keywords: Critical pore length; Pore space microstructure transitions; Pore-level flow; Permeability–porosity relation

1. Introduction

As our conceptual understanding and numerical expertise to simulate more and more complex flow and transport systems increase, the accuracy of current simulations hinges on the quality and completeness of input and system parameters. This is true in modeling flow in oil and gas rocks, determining flow in underground reservoirs and fate of chemical contaminants in the vadose zone, assessing the effectiveness of leaching processes, and optimizing filtration and sedimentation operations. For a broad range of applications, the most important transport property of porous media is permeability. Until the 1980s, numerous relations between permeability (k) and porosity (ϕ) were proposed, starting with the Kozeny–Carman relation based on capillary tube models [1,2], however all seem to lack universality and predictability. For a review of the history of the k–ϕ relationships, see for instance, [3]. In the 1980s, the diagenetic origin of rock pore space and the geometric-topologic similarities between sedimentary rocks led Katz and Thompson (K&T) [4] to the idea than certain common elements of pore formation may

* Corresponding author. Tel.: +56 41 204534; fax: +56 41 247491.
E-mail address: petoledo@udec.cl (P.G. Toledo).

1385-8947/$ – see front matter © 2005 Published by Elsevier B.V.
doi:10.1016/j.cej.2005.02.003

be universal and as such may be described by a fundamental growth model. In 1986 the same authors proposed an approach to flow in porous rocks leading to accurate descriptions of permeability and electrical conductivity of sandstone rocks [5]. In their approach permeability is related to the formation factor of the rock through a single effective pore diameter measured from a mercury injection experiment, but not directly to the porosity. K&T permeability relation have probed valid for essentially all porous rocks and for a broad class of porous media. Since their introduction the method has seen growing recognition, although the pressure and temperature dependence of properties yet have not been examined with the model. Considering that in situ properties at elevated pressure and temperature are often the most relevant rock properties, the existence of unexplained experimental data on properties of porous media under compaction, and the question on the capability of the K&T relation to describe in situ conditions recently led Rozas [6–8] to study the k–ϕ relationship of porous materials under compaction. Experimental permeability–porosity data of porous rocks and some other materials under compaction reveal at least three types of behavior: (1) permeability scales with porosity with a unique exponent in the entire porosity range, (2) permeability shows one scaling at high porosity and another in the neighborhood of a critical porosity threshold ϕ'_c in which the transport properties decay steeply, and (3) the scaling of permeability with porosity in a given material is valid only by porosity ranges. Examples can be found in permeability data for Fontainebleau sandstone [9], fused glass spheres [10], sintered glass beads, resin-cemented glass beads and several reservoir sandstones [11], hot-pressed calcite [12], and fiber filters and pressed fiber mats [13]. All these behaviors are well explained by Rozas [6–8], at the center are first-order pore microstructure transitions very well tracked by the K&T effective pore length. Rozas [6–8] has shown that Monte Carlo permeability data from two- and three-dimensional networks under compaction may not always follow the K&T relation.

Here we study the k–ϕ relationship in two-dimensional networks with a shrinking tube model using stationary flow simulations of an incompressible fluid. Special attention is placed on pore space microstructure transitions during shrinking. Monte Carlo (MC) simulations on large networks and lattice Boltzmann (LB) calculations are used to determine permeability as the shrinking process advances. New graphical representations of k/l_c^2 versus $\phi - \phi'_c$ for the various porosity intervals display straight and parallel lines, with a slope of 1, confirming that a universal relationship between k/l_c^2 and ϕ should not be discarded.

2. Pore space model

2.1. Pore network

We use two-dimensional square networks of rectangular bonds, or tubes, and nodes as underlying lattices. The hydraulic conductance of rectangular tubes, with length l and regular square cross sections circumscribing circles of radius r, is $g = \pi r^3/8\mu l$, where μ is the fluid viscosity. Nodes have infinite conductance. A uniform pore tube radius distribution between 1 and 2 μm, which we called $U(1, 2)$, is used for decorating the underlying lattices for predictions of permeability as a function of porosity.

2.2. Pore shrinkage

In the usual bond-percolation problem, the radius or the conductance of an element chosen at random is set to 0. Repetition of this procedure results in a finite conduction threshold p_c for the conductive network. Below p_c the network becomes disconnected and ceases to conduct. The formation of a sedimentary rock and the consolidation of particles during a sedimentation process, however, follow a different process. Regardless of the overburden pressure exerted on a given porous material or the number, size, and shape of particles deposited on pore walls, the probability of a pore becoming completely sealed to fluid flow is very small. In 1984, Wong et al. [14] introduced a random bond-shrinkage mechanism by which the porosity of a porous material can be varied (decreased) in much the same qualitative way as real rocks and sediment structures do. The interesting feature of this simple diagenetic model is that it has zero p_c. Here we use this model to study pore space variations with porosity and the impact on permeability. In Wong's model a tube is selected at random and its radius (or conductance) is reduced by a fixed shrinking factor λ, $r_i \rightarrow \lambda r_i$ where $0 \leq \lambda < 1$, this process is repeated until ϕ is reduced either to zero or a preset value. The length of the pores l remains unchanged during the shrinking process. Since ϕ and k of a rectangular tube are proportional, respectively, to r and r^3, they decrease, respectively, by a factor of λ and λ^3. We neglect the nodes at which the tubes meet. The model has three attractive features: (i) preserves the network connectivity for any $\lambda > 0$ in the $\phi = 0$ limit, (ii) the amount of change in r_i at any step of the simulation depends on the value of r_i at that time, and (iii) the limit $\lambda = 0$ corresponds to the classical percolation problem.

2.3. Effective pore length or critical pore size

The critical path of a conductive material is set by the cluster of pores offering the smaller resistance to transport through the material [15]. The pressure ΔP_c needed for the formation of an infinite conductive cluster defines an effective pore length or critical pore size l_c for the entire medium [5]. l_c represents the smallest pore size such that the set of pore sizes greater than l_c still forms and infinite, connected cluster. l_c is determined here in each stage of the shrinking process by MC simulation of mercury injection experiments.

In rectangular pores $l_c = \gamma \cos\theta/\Delta P_c$, where γ is 485 dyn/cm for mercury and θ measured through the mercury phase is 130°.

3. Flow models

3.1. Monte Carlo

The distribution of nodal potentials in a "decorated" lattice or pore network with any level of porosity is calculated by an iterative solution of Kirchhoff's equations of current conservation at nodes. A nodal fluid material balance leads to a system of linear equations, $\mathbf{Gp} = \mathbf{b}$, where $\mathbf{G}$ is a matrix of pore tube conductances, $\mathbf{p}$ is a vector containing the unknown pressures, and $\mathbf{b}$ is a vector depending on the pore pressures at the network upper and lower boundaries and the conductances of the pore tubes connected to these boundaries. For example, in two dimensions for a square network, a typical material balance in a node leads to

$$\begin{aligned} &g^X(x, y)P(x-1, y) + g^Y(x, y)P(x, y-1) - [g^X(x, y) \\ &\quad + g^Y(x, y) + g^X(x+1, y) + g^Y(x, y+1)]P(x, y) \\ &\quad + g^X(x+1, y)P(x+1, y) \\ &\quad + g^Y(x, y+1)P(x, y+1) = 0, \\ &x = 1, \ldots, n_X, \quad y = 1, \ldots, n_Y \end{aligned} \tag{1}$$

where (x, y) represents the position of the node inside the network, $g^X(x, y)$ is the conductance of an X-directed pore segment connecting nodes (x, y) and $(x-1, y)$, $g^Y(x, y)$ is the conductance of a Y-directed pore segment connecting nodes (x, y) and $(x, y-1)$, $P(x, y)$ is the pressure at node (x, y) and n_X and n_Y are the number of nodes in the X and Y directions, respectively. To find the distribution of nodal pressures in the fluid phase network once an external pressure gradient is imposed we use an iterative solution of the system of equations. The Monte Carlo results presented here are obtained with the conjugate gradient method preconditioned by symmetric successive over-relaxation (SSORCG). This method is part of the ITPACK routine libraries publicly available at the web site http://rene.ma.utexas.edu/CNA/ITPACK. ITPACK requires sparse matrix storage. For percolating systems a preliminary reduction is applied before solving the system of linear equations. The method of "burning" of Herrmann et al. [16] is used to determine the sample-spanning cluster and then, the connected cluster or current-carrying backbone. A bond is not part of the backbone if for topological reasons it is unable to carry current, i.e., if it is part of a dangling end. After such bonds are eliminated, the remaining system of equations is solved with SSORCG method. With the nodal potentials of the fluid phase network in hand, the flow rate everywhere can be determined, and the network conductance in a particular direction computed from Darcy's law [17,18], i.e., $g_{\text{Net}} = Q/\Delta P$ where Q is the total flow rate through the network and ΔP is the pressure difference across the network. The corresponding permeability is $k = g_{\text{Net}}\mu L/A$, where μ is the fluid viscosity, and L and A are, respectively, the length and width of the pore network.

3.2. Lattice Boltzmann

The LB method is a numerical scheme for simulating fluids with complex interfacial dynamics and boundaries [19–23]. Unlike conventional numerical schemes based on discretization of macroscopic continuum equations, the LB scheme is based on microscopic models and mesoscopic kinetic equations. The key idea is to construct simplified kinetic models incorporating the physics essentials so that the macroscopic averaged properties obey the desired macroscopic equations. In the LB method average fluid particle populations replace discrete fluid particles. The mean populations move from node to node on a regular lattice, and are redistributed at each time step by a collision operator which conserves mass, momentum and energy. There are a number of ways for implementing a suitable collision operator. A simple approach is to apply a relaxation to each population N_i with a time constant $1/\omega$, this leads to the single relaxation time Boltzmann method or BGK-Boltzmann method [23], named after Bhatnagar et al. [24], i.e.,

$$N_i = (\mathbf{x} + \mathbf{c}_i, t + \Delta t) - N(\mathbf{x}, t) = -\omega(N_i - N_i^{\text{eq}}) \tag{2}$$

where $N_i(\mathbf{x}, t)$ is the mean particle population located at lattice site $\mathbf{x}$ at discrete time step t and moving with velocity $\mathbf{c}_i$ towards the neighboring lattice site located at $\mathbf{x} + \mathbf{c}_i$. Eq. (2) is known as evolution equation. The right-hand side of Eq. (4) represents the collision between particles or the BGK relaxation with time constant $1/\omega$ towards the local equilibrium population N_i^{eq}. N_i is a specific function of the local density and the local velocity. The parameter ω is chosen to achieve the desired kinematic viscosity of the fluid, i.e., $\nu = (2/\omega - 1)/6$, ω determines all transport properties of the resulting fluid. The scheme is linearly stable for $0 < \omega < 2$. Each evolution cycle, corresponding to one integration step of the LB method, consists of one advection and one relaxation. The above formalism leads to a velocity field that is a solution of the Navier–Stokes equations [22].

No-slip wall conditions are implemented by imposing bounce-back-reflection of the populations N_i at solid walls [25,26]. For the simulations here, flow is started from a zero velocity at each node in the computational domain. A pressure gradient or forcing factor drives the fluid. A uniform force density in the fluid represents this gradient here [25,26]. To approximate infinitely long media, periodic boundaries are imposed on pore network sides open to flow. Lateral network sides are impervious.

In two-dimensional simulations, we consider an orthogonal lattice with eight moving populations and one rest population to represent the fluid domain. The orthogonal 9-speed model is abbreviated by the symbol D2Q9 following the convention of Qian et al. [22]. The equilibrium populations for the D2Q9 model are given by the following equations [22]:

$$N_i^{\text{eq}} = \tfrac{1}{36}\rho[1 + 3(\mathbf{c}_i \cdot \mathbf{u}) + \tfrac{9}{2}(\mathbf{c}_i \cdot \mathbf{u})(\mathbf{c}_i \cdot \mathbf{u}) - \tfrac{3}{2}(\mathbf{u} \cdot \mathbf{u})] \tag{3}$$

for the populations moving along the diagonal directions:

$$N_i^{eq} = \frac{1}{9}\rho[1 + 3(\mathbf{c}_i \cdot \mathbf{u}) + \frac{9}{2}(\mathbf{c}_i \cdot \mathbf{u})(\mathbf{c}_i \cdot \mathbf{u}) - \frac{3}{2}(\mathbf{u} \cdot \mathbf{u})] \quad (4)$$

for the populations moving along the vertical and horizontal directions, and

$$N_i^{eq} = \frac{4}{9}\rho[1 - \frac{3}{2}(\mathbf{u} \cdot \mathbf{u})] \quad (5)$$

for the non-moving populations.

The fluid density $\rho(\mathbf{x}, t)$ and velocity $\mathbf{u}(\mathbf{x}, t)$ are calculated from the populations N_i, respectively, through the relations $\rho(\mathbf{x}, t) = \sum_{i=0}^{8} N_i(\mathbf{x}, t)$ and $\mathbf{u}(\mathbf{x}, t) = (1/\rho(\mathbf{x}, t))\sum_{i=1}^{8} Ni(\mathbf{x}, t)\mathbf{c}_i$. As in previous work [26], we select $\omega = 1.85$ for all the simulations discussed in this work.

Once the steady state is reached, the fluid permeability is calculated using Darcy's law [17,18], i.e., $\mathbf{u} = -(k/\mu)\nabla P$, where ∇P is the macroscopic applied pressure gradient.

4. Results and discussion

Pore size distribution and pore space connectivity are fundamental for a suitable geometric-topologic representation of porous materials. Pore space connectivity should not be very sensitive to shrinking or compaction unless the process is severe. In this work, the idealization is used that the pore space connectivity remains unchanged except when the deformation process leads to pore closing. Fluid topology however does change significantly even when shrinking is no that severe. Thus, for a fixed pore space connectivity, the macroscopic bulk- and single-phase transport properties in a particular state of the system, i.e., fluid topology, are defined from its pore size distribution function. From here derives our interest in studying the evolution of this function in pore networks subject to shrinking processes of controlled intensity.

Porous materials can be classified according to the characteristics of their pore populations before and during shrinking. Some materials display a noticeably wide distribution of pore sizes, they are heterogenous; others however have a narrow distribution, i.e., they display a relatively small degree of heterogeneity. Another characteristic is the degree of asymmetry of the distribution or skewness that reveals coexistence of pore populations with significantly different size. One of these populations, generally the largest, controls the macroscopic properties of the material. Some materials however exhibit a somewhat uniform distribution; for these it is difficult to establish a characteristic pore size controlling the macroscopic properties of the material because nearly identical pore fractions of each size coexist. The evolution of a distribution depends mainly on the elastic properties of the material and on the intensity of the shrinking process. In the simulations here the shrinking factor λ accounts for these two characteristics.

Fig. 1 shows an initial unperturbed two-dimensional square network of 12×25 nodes decorated with a uniform $U(1, 2)$ pore size distribution function. Fig. 2 displays the

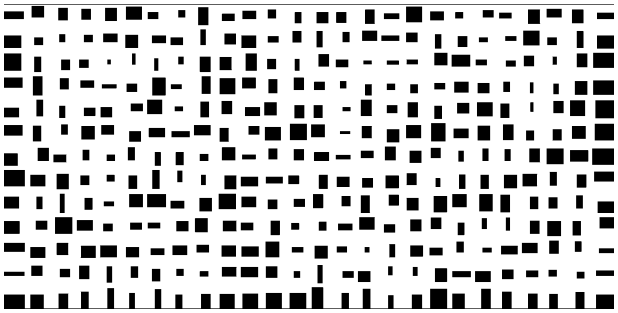

Fig. 1. Unperturbed two-dimensional square network of 12×25 nodes decorated with a uniform $U(1, 2)$ pore size distribution function.

evolution of pore space of the square network in Fig. 1 under various shrinking intensities ranging from weak to strong. Fig. 3 shows the evolution of the $U(1, 2)$ distribution, for larger networks of 1,000,000 pores, as shrinking of various intensities reduces pore size and thus porosity.

The $U(1, 2)$ distribution shows a smooth evolution when the pore network suffers smooth shrinking, i.e., for $\lambda = 0.99$, as Figs. 2 and 3a reveal. The distribution remains unimodal and asymmetrically centered around a mean pore size that decreases with shrinking. Fig. 3a shows increasing asymmetry of the distribution at early stages of the shrinking process; such asymmetry decreases markedly towards the end of the process. This result is suggestive of pore spaces able to conserve their original structural characteristics under smooth shrinking (see Fig. 2 for $\lambda = 0.99$). It is highly probable that real porous materials under this kind of deformation show no significant pore structural differences, beyond the obvious porosity change, in two stages of its shrinking history. Nevertheless, the sole observation of the evolution of the distribution is not enough to establish definitive conclusions. Later we see that the effective pore length of each medium, which fixes the scale of permeability, is the key property to determine the existence of porous microstructure transitions as shrinking advances.

The situation changes significantly when the shrinking occurs with greater intensity, here characterized by small values of λ. Fig. 3b–e shows that the $U(1, 2)$ distribution evolves towards a multimodal function as a result of the appearance of new populations of smaller-sized pores which coexist with part of the primitive pore population of the material. The initial pore population diminishes with shrinking but conserves its original shape. The size distribution of these pores remains unimodal and centered symmetrically around the initial mean pore size; its standard deviation increases at the beginning of the shrinking and diminishes towards the end of the process. The new pore populations or modes of the size distribution grow at expenses of the larger-sized pore populations. The shape of these new modes is a replica on smaller scale of the mode feeding them. A pore population or mode appears, grows, reaches a maximum size, decreases, and disappears with shrinking. The separation of pore populations is more pronounced for the case of shrinking with $\lambda < 0.3$. The ex-

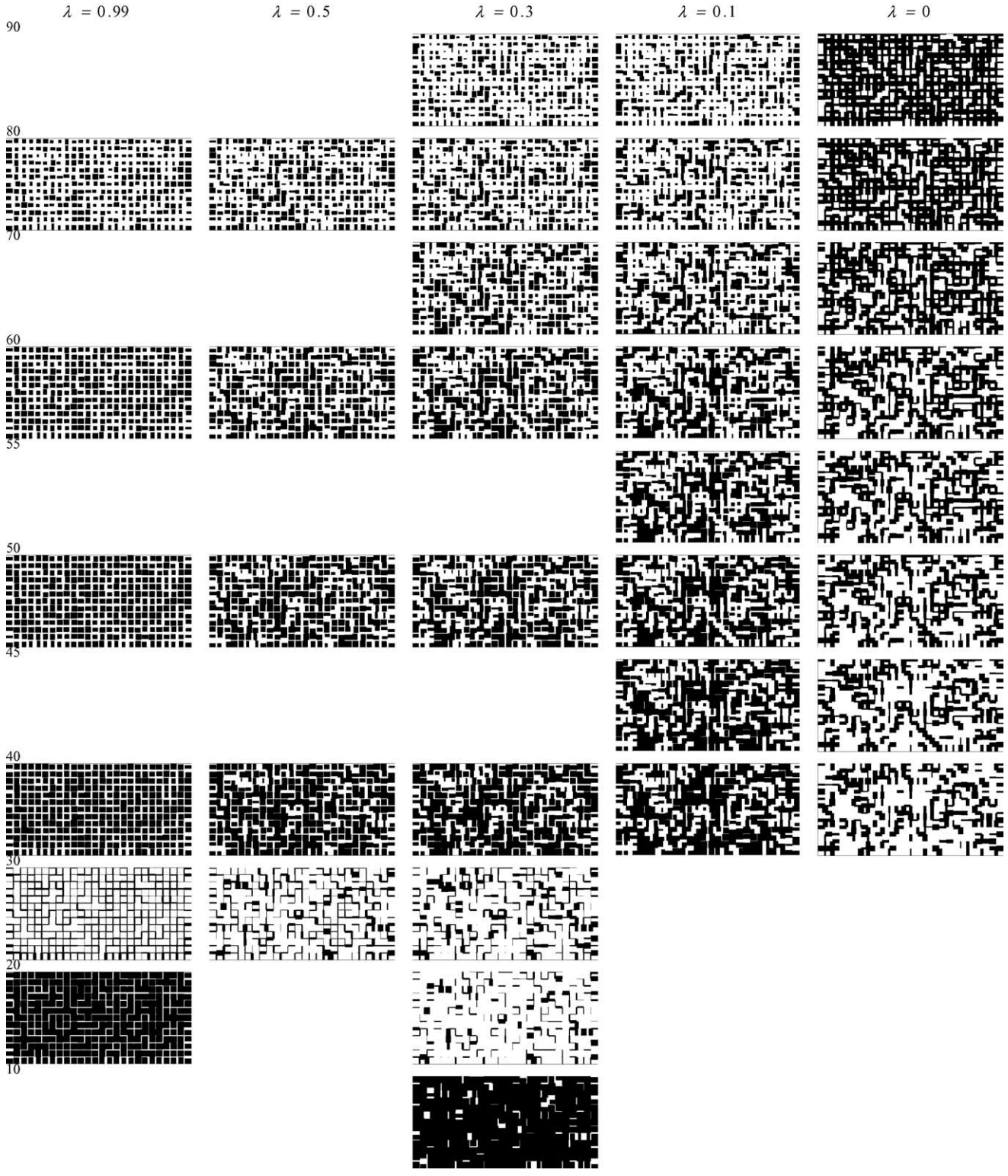

Fig. 2. Sequences of pore space microstructures for two-dimensional square networks undergoing shrinking. Network size is 12 × 25 nodes. Pore size distribution of the unperturbed network (Fig. 1) is a uniform $U(1, 2)$ function. Shrinking factors from left to right are 0.99, 0.5, 0.3, 0.1, and 0. Relative porosities for microstructure images on a given file are indicated at the left.

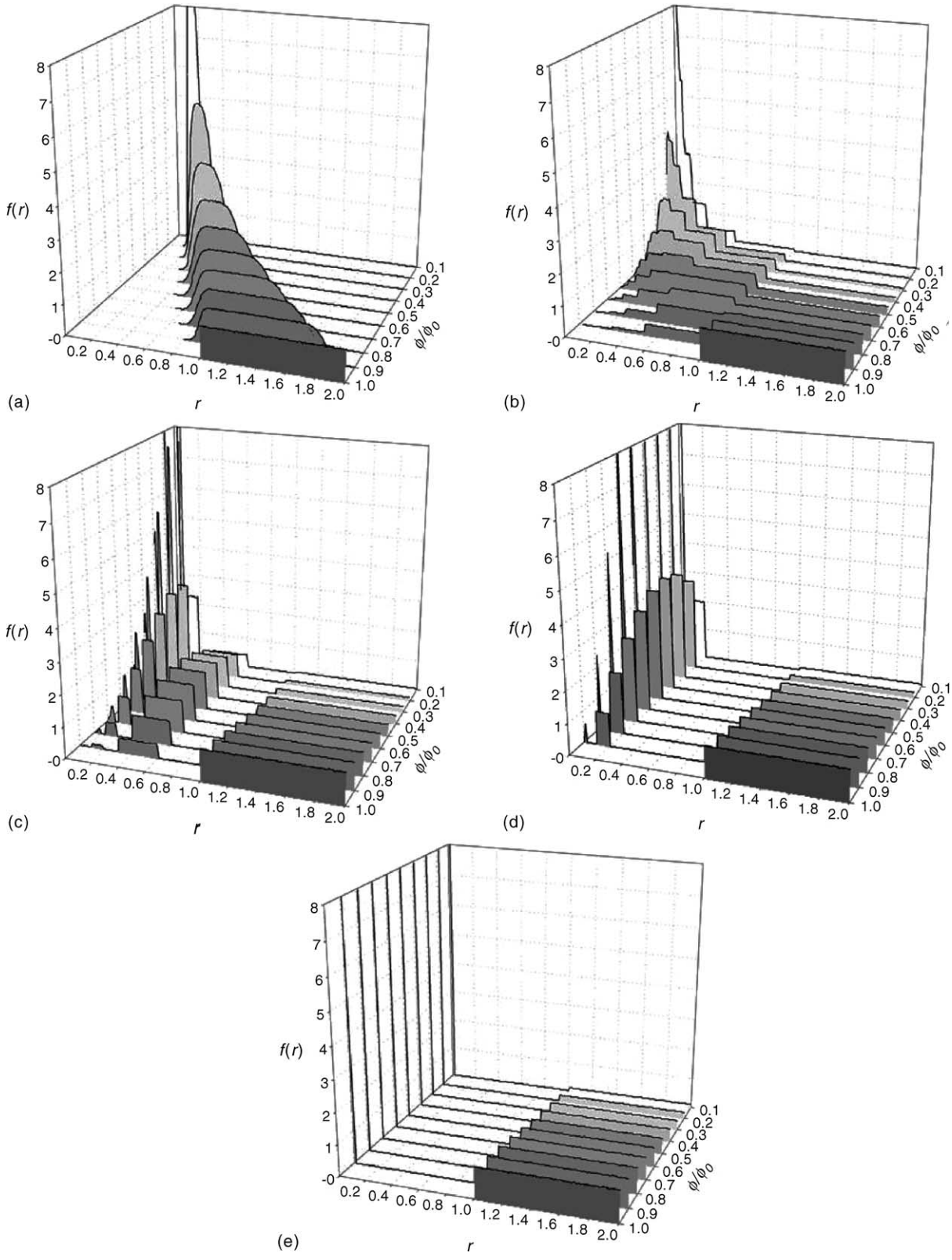

Fig. 3. Evolution of a uniform $U(1, 2)$ pore size distribution in a large two-dimensional square network for a range of shrinking factors (a) 0, (b) 0.1, (c) 0.3, (d) 0.5, and (e) 0.99.

treme case for $\lambda = 0$, Fig. 3e, corresponds to the classic percolation process; the net effect is the split of the initial pore population in two, one for the open pores and another for the closed pores. According to these results, pore spaces are unable to conserve their original structural characteristics when exposed to severe deformation processes as Fig. 2 shows for small values of λ. Porous materials at contiguous levels or stages of this type of shrinking may show differences beyond the porosity if different pore populations dominate their distributions of pore sizes, the definitive answer for each pore network is obtained from the evolution of the effective length with shrinking.

Shrinking is defined as strong or intense when it causes radical changes in the porous microstructure of a material. The behavior of wide pore size distributions is different from that exhibited by narrow distributions for the same shrinking factor when this value is small [6,7]. Thus, the value of the shrinking factor alone is insufficient to conclude respect to the intensity of a shrinking process. The intensity is defined mainly by two aspects: the elastic properties of the material and the force applied on the material, these two define the shrinking factor λ and the width of the initial pore size distribution. Thus, for two materials presenting distributions of different width but of equal minimum pore size it is more likely that shrinking processes produce new modes in the narrowest distribution for the same λ. This effect has important consequences on the behavior of the transport properties of pore networks since if some of these new modes with smaller pores dominate the total pore population then the material may suffer a transition in its porous microstructure.

Fig. 4 shows the evolution of the single effective or critical pore length of large two-dimensional networks subject to shrinking processes from weak to strong. l_c is calculated from MC simulations of mercury injection experiments. l_c and ϕ are displayed normalized respect to the properties of the unperturbed networks. Networks are 600×600 nodes decorated with the uniform pore size distribution $U(1, 2)$.

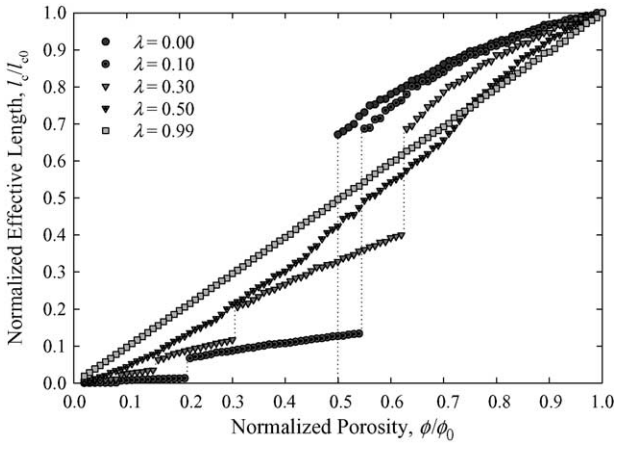

Fig. 4. Effective pore length vs. porosity for a two-dimensional square network decorated with the initial $U(1, 2)$ pore size distribution for various shrinking factors.

The results in Fig. 4 suggest that weak shrinking, $\lambda = 0.99$, produces media resembling the unshrinked original media, i.e., all the important details of the media remain; l_c evolves continuously as ϕ is decreased with shrinking. An observer of the medium at any level of ϕ, beyond the obvious reduction of ϕ, would not perceive significant geometric-topologic changes in the pore space respect to the original space. The porous microstructure retains its characteristics throughout the shrinking process. Fig. 3a support this idea, pore size distribution remains unimodal and the shrinking effect is limited to reducing porosity. In other words, the porous microstructure "remembers" its primitive form. From a geophysical point of view what we called weak shrinking is simply a smooth diagenetic process that reduces ϕ, the class however remains unchanged; for instance a sandstone continues being a sandstone although with smaller porosity. It is worth mentioning that the reduction of ϕ from 1 to 0 for the smooth shrinking ($\lambda = 0.99$) is possible only within the framework of the proposed model. In fact a smooth shrinking regime reduces ϕ of a material until a finite limit different from zero, but in the process the porous microstructure retains the characteristics of the primitive material.

As shrinking intensity increases, the case of $\lambda = 0.5$ in Fig. 4, the behavior of l_c becomes erratic, with numerous and thus far unknown inflections. Fig. 3b suggests these inflections are consequence of the appearance of new pore size distribution modes dominating the original single-mode pore size distribution and thus the porous medium geometric properties. As shrinking intensity increases, $\lambda < 0.5$, these inflections in l_c result in discontinuities revealing clear pore space microstructure transitions.

The results in Fig. 4 for strong shrinking regimes, $\lambda < 0.3$, reveal clear transitions in l_c as ϕ decreases with shrinking. l_c is continuous by parts only, exhibiting transitions at finite critical porosities, pseudo-critical strictly. These transitions are associated with strong changes in the distribution of pore sizes, including the appearance of new modes in the distribution as Fig. 3c–e shows. Continuous pieces of l_c correspond to structurally different porous media. A discontinuity marks a transition from a more "open" porous microstructure to a more "closed" one, the size of the pores controlling the transport properties of the latter decreases sharply. The new microstructure "forgets" its origin, its memory is only enough to remember the microstructure at the beginning of the continuous piece of l_c to which it belongs. From a geophysical point of view what we refer here to strong shrinking may be associated with strong diagenetic processes that not only reduce the porosity but also transforms one porous microstructure into another changing its class or lithology in the process. For example, the geophysical and geochemical transformation of a weakly cemented clean sand into a strongly cemented mineral-inclusion-rich sand changes a porous microstructure into a radically different one. As in the case of weak shrinking, the reduction of porosity from 1 to 0 and the multiple microstructural transitions of pore space for strong shrinking are possible only within the framework of the model. Actually

Table 1
Pseudo-critical porosities at which l_c becomes discontinuous for a two-dimensional square network decorated with the initial $U(1, 2)$ pore size distribution for various shrinking factors

Shrinking factor λ	Pseudo-critical porosities		
	1st inflection	2nd inflection	3rd inflection
0	0.5	–	–
0.1	0.5362	0.2230	0.0924
0.3	0.6157	0.3107	0.1600
0.5	0.7071	0.4322	0.2637
0.99	–	–	–

a strong compaction regime reduces the porosity of a material until a finite limit different from zero, but in the process it can produce one or more transformations of microstructures. The strong shrinking produces richly connected pore spaces at high porosity and poorly connected ones at low porosity.

Table 1 presents the first three pseudo-critical porosities, see Fig. 4, at which discontinuities in l_c occur. Discontinuities are clearer as $\lambda \to 0$, i.e., when shrinking is strong.

The effective pore length of a porous material and its transitions during a shrinking process are closely related to the permeability of the material, and its pursuit allows to establish a clear distinction between highly deformable and weakly deformable materials. This new transition, apparently of first order, that finds support in experimental data in the literature, was first identified by Rozas [6,7]. From Fig. 4 it is easy to establish an analogy between the transition of porous microstructures and for instance the first-order transition in fluid phases. Finally, after observing the non-trivial behavior of l_c of pore networks during shrinking, especially its capacity to respond to microstructural changes, Rozas concluded that it is the appropriate length scale to predict permeability and other porous media transport properties. To the light of these results neither the hydraulic pore diameter nor the length lambda [27], based on electrical measurements, are able to capture the wealth and complexity of pore spaces undergoing microstructural transitions.

Next we present results of the evolution experienced by the permeability of pore networks as the pore space is shrinked. In the cases studied the results of MC simulations are compared with estimations based on the LB method. The MC simulation results are based on large square networks of 250 × 250 nodes. The LB calculations are based on smaller square networks of 12 × 25 nodes. The correct performance of the LB scheme employed here has been tested with several numerical experiments (see [28] for details). Fig. 5 shows the sensitivity of the LB permeability of two-dimensional square networks of 12 × 25 nodes to factors such as forcing (Fig. 5a) and pore space discretization (Fig. 5b). Results in these figures correspond to the unperturbed network in Fig. 1. For this network the optimum forcing factor and lattice discretization are 0.05 and 2030 (along the main flow) × l014, respectively. Results show that lower porosity networks are more demanding on discretization for a correct representation of flow therein.

Fig. 6 presents a comparison of MC and LB permeability–porosity data for square networks decorated with an initial narrow distribution of pore size $U(1, 2)$ for five shrinking factors, i.e., $\lambda = 0$, 0.1, 0.3, 0.5 and 0.99. In all cases of λ, the LB permeability tracks the MC k–ϕ curve extremely well.

Fig. 6a shows that for $\lambda = 0.99$ the permeability of the square network follows a simple power-law type dependency with the porosity, that is, $k \propto \phi^m$. A single value of m suffices to describe the relation k–ϕ for any porosity in this type of shrinking. The value for this exponent is $m = 3$, the Kozeny–Carman limit. A close inspection of Fig. 6b shows that for $\lambda = 0.5$ more than one value of m is necessary to describe the k–ϕ relation. For the high porosity range, between the pseudo-critical porosity $\phi_c = 0.7071$ (see Table 1 and Fig. 4) and $\phi = 1$, again the exponent is $m = 3$. For lower porosities, below $\phi_c = 0.7071$, $m > 3$. Similar is the situation for $\lambda = 0.3$ in Fig. 6c, the lower value for the exponent is $m = 3$ and occurs in the high porosity range between the pseudo-critical porosity $\phi_c = 0.6157$ (see Table 1 and Fig. 4) and $\phi = 1$. The inflections at lower porosities in Fig. 6b and c

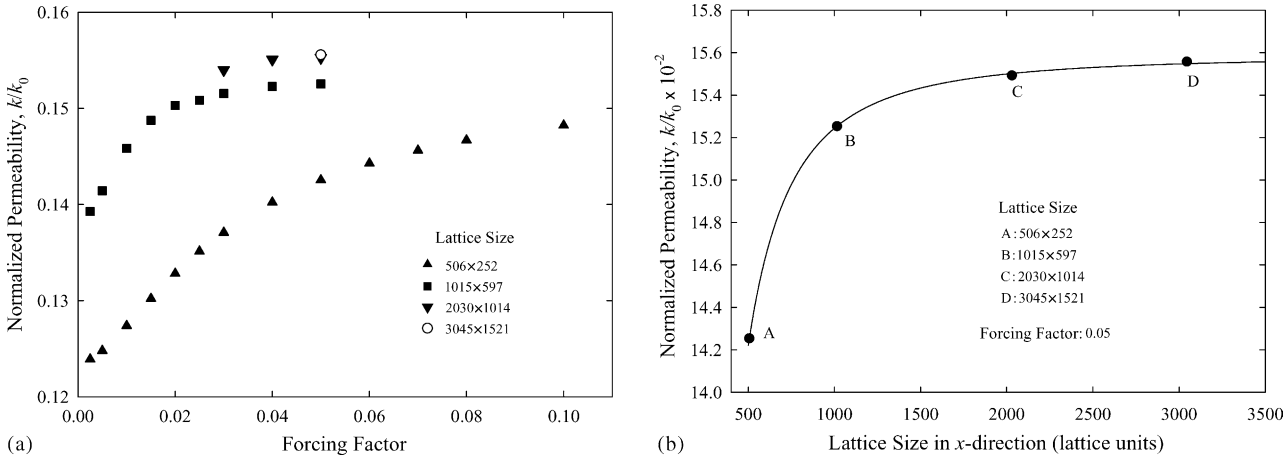

Fig. 5. Sensitivity of lattice Boltzmann permeability of two-dimensional square networks of 12 × 25 nodes to (a) forcing factor for various lattice sizes and (b) lattice size for forcing factor 0.05.

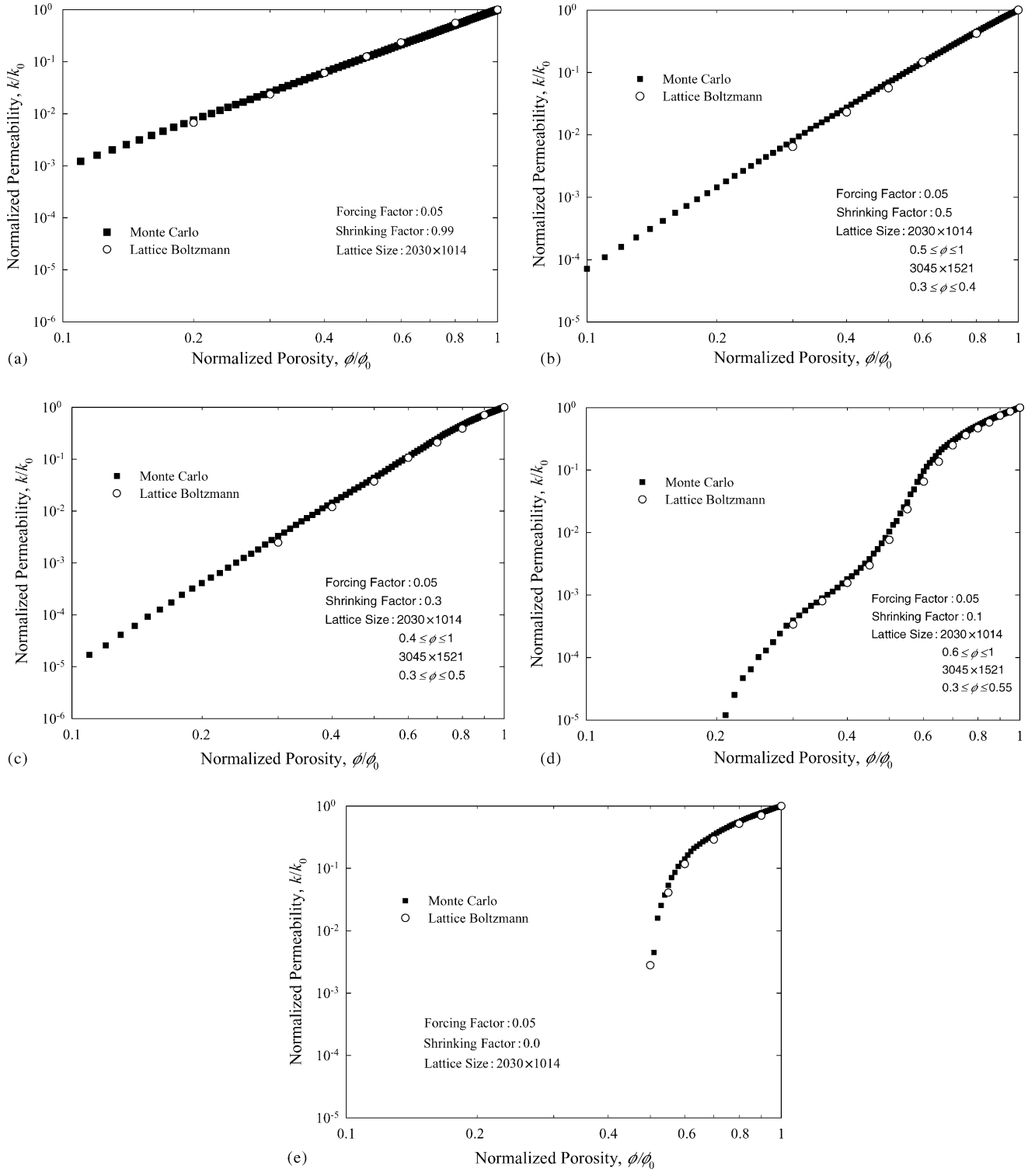

Fig. 6. Permeability–porosity data for two-dimensional square networks undergoing shrinking. Comparison of Monte Carlo and lattice Boltzmann results. The initial pore radii distribution is $U(1, 2)$. Shrinking factors are (a) 0.99, (b) 0.5, (c) 0.3, (d) 0.1, and (e) 0.

are not first-sight apparent. For $\lambda = 0.1$ however a nonlinear behavior of the permeability curve in Fig. 6d is clear. The inflection point at the relatively high pseudo-critical porosity, $\phi_c = 0.5362$ is a consequence of different pore populations controlling permeability in different stages of the shrinking process. Inflection points at lower porosities than $\phi_c = 0.5362$ are not shown in Fig. 6d. More than one value of m is necessary to describe the k–ϕ relation, the lower value is $m = 3$ and, as expected, occurs when porosity tends to 1. As mentioned before, the narrow distribution $U(1, 2)$ shows multiplicity of

modes or pore populations for $\lambda = 0.1$ (Fig. 3d), which in principle explains the inflection points and the existence of different porous microstructures before and after these points. Fig. 6d shows that for $\lambda = 0$ the behavior of permeability is that of the transport properties in the classic percolation problem, the novelty being that the critical point for all the cases studied in the square network occurs at a normalized porosity, equal to 0.5, identical to the percolation threshold p_c in the same network. The same occurs in the case of the electrical conductivity [6]. When the pore volume of the network has been reduced in a 50%, an infinite conductive cluster of pores does not exist, and implies necessarily that half of the connections have been eliminated. We have proved that when $\lambda = 0$ the normalized porosity is exactly equal to the fraction p of conductors in the square network. Qualitatively, when $\lambda = 0$ the shrinking is equivalent to a random elimination of bonds in the network. It is a percolation process and thus the conductor–insulator transition state of the network, which is independent of the distribution of pore sizes, the definition of the conductance elements, and of some other details, depends exclusively on the dimensionality of the network. In Fig. 6e, the lower value for the exponent in the relation $k \propto \phi^m$ is $m = 3$ and, as expected, occurs when porosity tends to 1.

An important body of experimental permeability data for diverse classes of porous materials under compaction shows the beginning of a permeability inflection or transition, i.e., the change that occurs when one porous microstructure controlling permeability lets a new microstructure assumes this function. In general, the literature has denied physical sense to the steep reduction of permeability in the proximity of an inflection point. In most cases the data measured is not reported, and when reported are explained as being measured in the zone were they are not reliable. In the need to fit a power-law relation of the kind $k \propto \phi^m$, permeability data in the zone of steep decay are simply discarded. In some cases the relation $k \propto \phi^m$ is adjusted by porosity sections. Recently Mavko and Nur [10] adjusted the relation $k \propto (\phi - \phi_c)^3$ to various sandstones with remarkable success, ϕ_c is a pseudo-critical porosity acting as a fitting parameter. Mavko and Nur nevertheless do not provide a physical meaning for ϕ_c, they do not recognize the existence of an effective length of the pore space and even less suggest the existence of an inflection point to lower porosity than ϕ_c in the permeability curves examined. On the simulation ground, Wong et al. [14] could not calculate permeability for $\lambda < 0.25$ with the shrinking tube model and thus missed the transitions completely. The macroscopic properties of pore networks are related next through scaling laws.

First we consider the K&T relation [5] between permeability, formation factor F and effective length, i.e.,

$$k = c_1 k_0 \frac{l_c^2}{F} \tag{6}$$

where $F \equiv \sigma_o/\sigma$, σ is the electrical conductivity of a porous medium saturated with fluid with conductivity σ_0. Eq. (6) was deduced for three-dimensional media, specifically rocks and consolidated sands [5].

Fig. 7 displays k versus $c_1 l_c^2/F$ for 2D square networks decorated with $U(1, 2)$ pore size distribution.

Results in Fig. 7 show that Eq. (6) is valid for $\lambda = 0.99$ in the entire porosity range and for $\lambda < 0.99$ only in the porosity range between the first pseudo-critical and 1 (see Figs. 4 and 6 and Table 1). For $\lambda < 0.99$, Fig. 7 displays a significant depart from the 45° line in the porosity range between 0 and the first pseudo-critical, exactly in the region not studied thus far. Fig. 7 emphasizes the need for better LB data, particularly at low porosity. Rozas [6–8] have shown for various network dimensionalities, pore size distributions and shrinking factors that all $k - c_1 l_c^2/F$ curves show the same behavior as in Fig. 7. The prefactor in Eq. (6) is $c_1 = F_0/l_{c0}^2$, calculated in the $\phi \to 1$ limit. The results in Fig. 7 are important because they test for the first time the universality of the K&T relation. The practical importance of this result is easy to anticipate. When Eq. (6) applies, the only parameter of this relation, c_1, has physical meaning and can be determined with a single experimental k–ϕ data point.

According to the discussion above, a continuous section of l_c–ϕ curve corresponds to a porous microstructure that only reduces its porosity during a shrinking process. This microstructure controls the permeability of the material in that section. In the transition, the control of permeability switches from this microstructure to another. When the MC and LB results are represented in the form k/l_c^2 versus ϕ, see schematic in Fig. 8, a linear behavior is observed in the sections corresponding to each permeability regime, with slight deviations near the transition regions. That is, the following relation is valid for each porosity section,

$$\frac{k}{l_c^2} = c_2(\phi + b) \tag{7}$$

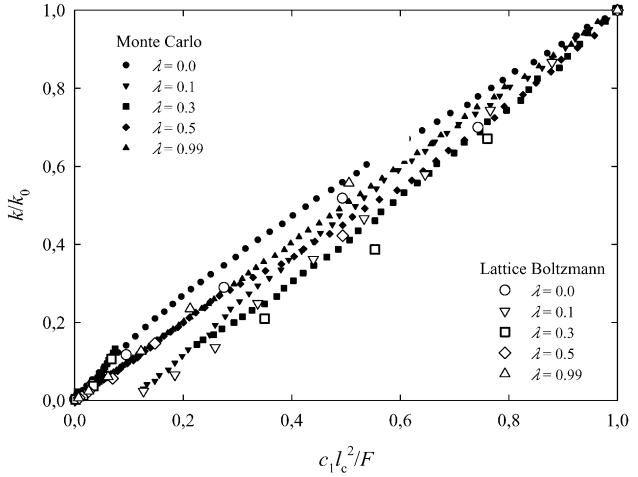

Fig. 7. Katz–Thompson permeability scaling for a two-dimensional square network decorated with an initial radii distribution $U(1, 2)$ for different shrinking factors.

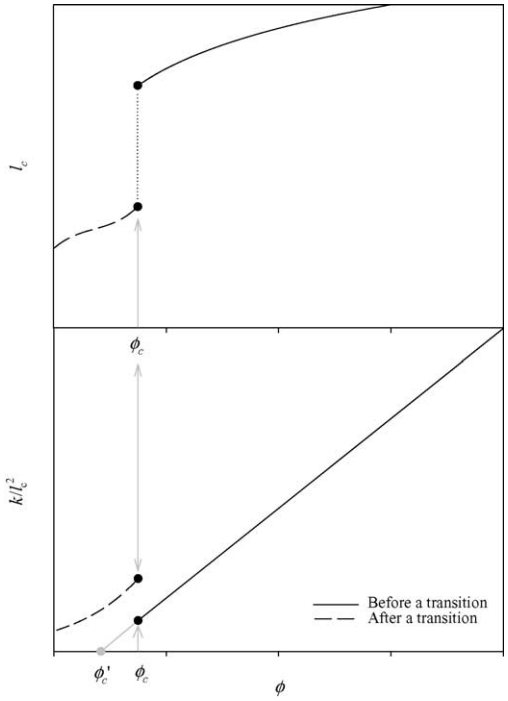

Fig. 8. Schematic representation of the method for determining pseudo-critical porosities at a given pore length transition.

where b is the k/l_c^2 intercept of this trial linear function. Now, if a given linear permeability regime is extrapolated until a hypothetical state of porosity for which permeability is zero, the result is $b = -\phi_c'$. That is, the term ϕ_c', here denominated pseudo-critical porosity, corresponds to the porosity of a hypothetical conductor–insulator transition that results from the extrapolation of the given permeability regime. The corresponding ϕ_c' for each permeability regime may be determine in the same manner.

Then, we postulate the following ansatz for the permeability:

$$\frac{k}{l_c^2} = c_2(\phi - \phi_c') \tag{8}$$

The prefactor in Eq. (8) is $c_2 = (k_0/l_{c0}^2)/(\phi_0 - \phi_c')$, where k_0, l_{c0}, and ϕ_0 pertain to the initial point and ϕ_c' to the pseudo-critical porosity of each permeability regime.

As it is shown in Fig. 9, Eq. (8) has universal character and is suitable for representing experimental data for each permeability regime or section. Rozas [6–8] has shown this character for various network dimensionalities, pore size distributions and shrinking factors.

Relation (8) is an alternative to the K&T relation to extrapolate and to interpolate permeability with certainty from experimental data. The parameters of this relation may be inferred from three experimental points; data on conductivity is not necessary. Fig. 9 emphasizes strongly the need for better LB data, particularly at low porosity and near pseudo-critical porosities.

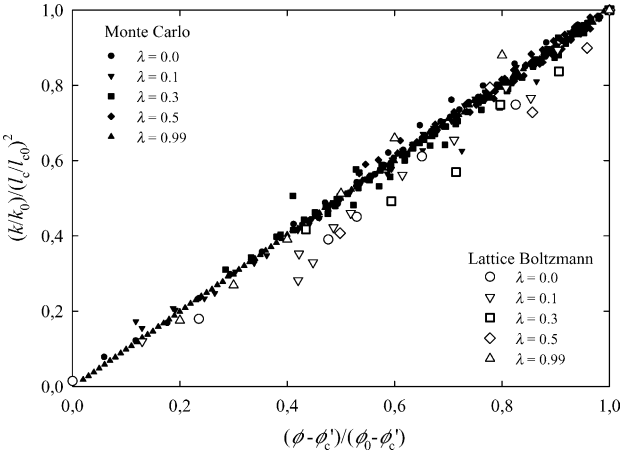

Fig. 9. Permeability scaling with porosity for a two-dimensional square network decorated with an initial radii distribution $U(1, 2)$ for different shrinking factors.

5. Conclusions

New graphical representations of k/l_c^2 versus $\phi - \phi_c'$ for various pore networks under shrinking display straight and parallel lines, with a slope of 1, suggesting that a universal relationship between k/l_c^2 and ϕ may be possible. At the hart are pore space microstructure transitions driven by the shrinking process. These transitions are associated with changes in the distribution of pore sizes, more precisely in the appearance of new modes in the distribution eventually controlling the transport properties. The new pore populations or modes of the distribution grow at expenses of the larger-sized pore populations. A pore population or mode appears, grows, reaches a maximum size, decreases and disappears with shrinking. Our results show that the old theory of Kozeny–Carman, derived for oversimplified porous media, contains some elements of the new k–ϕ. The problem is that the intrinsic limitations of the Kozeny–Carman relation have been increased by the need to fit scarce experimental data with aims of interpolating and extrapolating information. This need has remained for more than five decades and continues at present in spite of the clarifying works of Katz and Thompson [5], Wong et al. [14] and Roberts and Schwartz [29] by the end of the 1980s and beginning of the 1990s. Risky practices in the processing of permeability data include (1) the use of the theory of Kozeny–Carman with a constant effective length l_c along the entire process of permeability reduction, (2) the simple replacement of the l_c associated to the pore space by the mean size of particles or grains that conform the solid material if granular or of pseudo-grains if the solid material is consolidated with undefined grain, and (3) the extrapolation of permeability ignoring the existence of microstructure transitions. Results in the literature are varied, but in general when the adjustment of k–ϕ data is carried out by means of power-law relations using a constant l_c and avoiding a parameter of transition porosity, the sensitivity of the exponent to porosity is great. In some cases exponents from 3 to 8 are required

for a given material (see, e.g. [9]). These high exponents, to the light of the results presented here, are necessary because the data adjusted is in the vicinity of a permeability transition point. This situation is especially dangerous because implies extrapolation of permeability data, controlled by one type of microstructure, to a zone where permeability is controlled by a different microstructure.

Acknowledgments

Financial support from CONICYT-Chile through project FONDECYT No. 1030866 and from the Research Direction of University of Concepción through project DIUC 203.096.057-1.0 is greatly appreciated.

References

[1] J. Kozeny, Über Kapillare Leitung des Wassers im Boden, Sitzungsber. Akad. Wiss. Wien 136 (1927) 271–306.
[2] P.C. Carman, Fluid flow through a granular bed, Trans. Inst. Chem. Eng. London 15 (1938) 150–156.
[3] A.H. Thompson, A.J. Katz, C.E. Krohn, The microgeometry and transport properties of sedimentary rock, Adv. Phys. 36 (1987) 625–694.
[4] A.J. Katz, A.H. Thompson, Fractal sandstone pores: implications for conductivity and pore formation, Phys. Rev. Lett. 54 (1985) 1325–1328.
[5] A.J. Katz, A.H. Thompson, Quantitative prediction of permeability in porous rock, Phys. Rev. B 34 (1986) 8179–8181.
[6] R.E. Rozas, Permeabilidad de Medios Porosos: Experimentos Numéricos y Teoría, M.Sc. Thesis, University of Concepción, 2002.
[7] R.E. Rozas, P.G. Toledo, Pore space microstructure transitions as revealed by critical pore lengths, Phys. Rev. Lett., 2005, submitted for publication.
[8] J.R. Quispe, R.E. Rozas, P.G. Toledo, Permeability-porosity relationship from a geometrical model of shrinking and flow simulations in two-dimensional pore network, in: A.H. Reis, A.F. Miguel (Eds.), Applications of Porous Media, CGE, Portugal, 2004, pp. 15–25.
[9] T. Bourbié, O. Coussy, B. Zinszner, Acoustics of Porous Media, Gulf Publ. Co, 1987.
[10] G. Mavko, A. Nur, The effect of a percolation threshold in the Kozeny–Carman relation, Geophysics 62 (5) (1997) 1480–1482.
[11] W.J. Bosl, J. Dvorkin, A. Nur, A study of porosity and permeability using a lattice Boltzmann simulation, Geophys. Res. Lett. 25 (9) (1998) 1475–1478.
[12] Y. Bernabe, W.F. Brace, B. Evans, Permeability, porosity, and pore geometry of hot-pressed calcite, Mech. Mater. 1 (1982) 173–183.
[13] G.W. Jackson, D.F. James, The permeability of fibrous porous media, Can. J. Chem. Eng. 64 (1986) 364–374.
[14] P.-z. Wong, J. Koplik, J.P. Tomanic, Conductivity and permeability of rocks, Phys. Rev. B 30 (1984) 6606–6614.
[15] V. Ambegaokar, B.I. Halperin, J.S. Langer, Hopping conductivity in disordered systems, Phys. Rev. B 4 (1971) 2612–2620.
[16] H.J. Herrmann, D.C. Hong, H.E. Stanley, Backbone and elastic backbone of percolation clusters obtained by the new method of 'burning', J. Phys. A: Math. Gen. 17 (1984) 261–266.
[17] H. Darcy, Les Fontaines Publiques de la Ville de Dijon, Victor Dalmot, Paris, 1856.
[18] F.A.L. Dullien, Porous Media: Fluid Transport and Pore Structure, 2nd ed., Academic Press, USA, 1992.
[19] G.R. McNamara, G. Zanetti, Use of the Boltzmann equation to simulate lattice-gas automata, Phys. Rev. Lett. 61 (1988) 2332–2335.
[20] F.J. Higuera, J. Jimenez, Lattice gas dynamics with enhanced collisions, Europhys. Lett. 9 (1989) 663–668.
[21] H. Chen, S. Chen, W.H. Matthaeus, Recovery of the Navier–Stokes equations using a lattice-gas Boltzmann method, Phys. Rev. A 45 (1992) 5339–5342.
[22] Y.H. Qian, D. d'Humieres, P. Lalleman, Lattice BGK models for Navier–Stokes equation, Europhys. Lett. 17 (1992) 479–484.
[23] S. Chen, H. Chen, D. Martinez, W.H. Matthaeus, Lattice Boltzmann model simulation of magnetohydrodynamics, Phys. Rev. Lett. 67 (1991) 3776–3779.
[24] P.L. Bhatnagar, E.P. Gross, M. Krook, A model for collision processes in gases. I. Small amplitude processes in charged and neutral one-component systems, Phys. Rev. 94 (1954) 511–525.
[25] A.J.C. Ladd, Numerical simulations of particulate suspensions via discretized Boltzmann equation. Part 1. Theoretical foundation, J. Fluid Mech. 271 (1994) 285–310.
[26] A.J.C. Ladd, Numerical simulations of particulate suspensions via discretized Boltzmann equation. Part 2. Numerical results, J. Fluid Mech. 271 (1994) 311–340.
[27] D.L. Johnson, J. Koplik, L.M. Schwartz, New pore size parameter characterizing transport in porous media, Phys. Rev. Lett. 57 (1986) 2564–2567.
[28] J.R. Quispe, P.G. Toledo, Lattice Boltzmann simulations of flow through two-dimensional particle sediments, Int. J. Min. Process. 73 (2004) 91–102.
[29] J.N. Roberts, L.M. Schwartz, Grain consolidation and electrical conductivity in porous media, Phys. Rev. B 31 (1985) 5990–5997.